Middle ear dynamics in response to seismic stimuli in the Cape golden mole (*Chrysochloris asiatica*)

U. B. Willi[1], G. N. Bronner[2] and P. M. Narins[1,3,]*

[1]*Department of Physiological Science, UCLA, Los Angeles, CA 90095, USA, [2]Small Mammal Research Unit, Department Zoology, University of Cape Town, Cape Town, Republic of South Africa and [3]Department of Ecology and Evolutionary Biology, UCLA, Los Angeles, CA 90095, USA*

*Author for correspondence (e-mail: pnarins@ucla.edu)

Summary

The hypertrophied malleus in the middle ear of some golden moles has been assumed to be an adaptation for sensing substrate vibrations by inertial bone conduction, but this has never been conclusively demonstrated. The Cape golden mole (*Chrysochloris asiatica*) exhibits this anatomical specialization, and the dynamic properties of its middle ear response to vibrations were the subjects of this study.

Detailed three-dimensional middle ear anatomy was obtained by x-ray microcomputed tomography (μCT) at a resolution of 12 μm. The ossicular chain exhibits large malleus mass, selective reduction of stiffness and displacement of the center of mass from the suspension points, all favoring low-frequency tuning of the middle ear response. Orientation of the stapes relative to the ossicular chain and the structure of the stapes footplate enable transmission of substrate vibrations arriving from multiple directions to the inner ear.

With the long axes of the mallei aligned parallel to the surface, the animal's head was stimulated by a vibration exciter in the vertical and lateral directions over a frequency range from 10 to 600 Hz. The ossicular chain was shown to respond to both vertical and lateral vibrations. Resonant frequencies were found between 71 and 200 Hz and did not differ significantly between the two stimulation directions. Below resonance, the ossicular chain moves in phase with the skull. Near resonance and above, the malleus moves at a significantly larger mean amplitude (5.8±2.8 dB) in response to lateral *vs* vertical stimuli and is 180° out of phase with the skull in both cases.

A concise summary of the propagation characteristics of both seismic body (P-waves) and surface (R-waves) is provided. Potential mechanisms by which the animal might exploit the differential response of the ossicular chain to vertical and lateral excitation are discussed in relation to the properties of surface seismic waves.

Key words: hearing, vibration, hypertrophied malleus, subterranean, Chrysochloridae.

Introduction

The use of seismic signals, be it for inter- or intraspecific communication, for detection of prey or for orientation, has been reported in many different taxa in the animal kingdom, for example arthropods (Aicher and Tautz, 1990; Barth, 1982; Brownell, 1977; Cocroft, 2000; Michelsen, 1982), amphibians (Lewis and Narins, 1985; Narins, 1990), reptiles (Hartline, 1971) and mammals (Barnett et al., 1999; O'Connell et al., 1997; Rado et al., 1987; Randall and Lewis, 1997). The nocturnal foraging patterns of the Namib Desert golden mole, *Eremitalpa granti namibensis* (Fielden, 1991), and the animal's seismic environment (Narins et al., 1997) suggest that this species is capable of localizing sources of seismic disturbances at a distance (Mason and Narins, 2001, 2002; Narins et al., 1997; Lewis et al., in press). An anatomical specialization exhibited by some golden mole species, namely massively hypertrophied mallei (Von Mayer et al., 1995; Mason, 2003a), led Mason (1998, 2003b) to hypothesize that the mechanism underlying the detection of seismic signals is inertial bone conduction. Thus, owing to its inertia, the malleus moves less and/or out of phase with the skull in response to a seismic disturbance, resulting in relative motion between the skull and the ossicular chain and, consequently, excitation of the inner ear.

The Namib Desert golden mole exhibits unique foraging behavior whereby individuals move in statistically non-random patterns between localized prey sources (subterranean termite nests), which often involves walking on the sand surface with periodic head-dipping, presumably for sensing seismic cues (Narins et al., 1997). Given that these moles are both sightless and possess extraordinary middle ear anatomy, inertial bone conduction is a reasonable candidate for the mechanism

underlying seismic navigation. However, physiological evidence to support this idea has not been forthcoming because this species is protected in Namibia. We therefore chose another closely related species for this study, namely the Cape golden mole (*Chrysochloris asiatica*). This animal is abundant (and easily obtained) in a wide variety of soil types and habitats in the Western and Northern Cape Provinces of South Africa, including the Namaqualand coastal plain, where it is sympatric with *E. granti*. It also forages for invertebrates just below the soil surface, but sometimes also above ground, and exhibits similar middle ear specializations to *E. granti*. Whereas the malleus of *E. granti* is ball-shaped and that of *C. asiatica* is club-shaped (Mason, 2003a), both species possess highly hypertrophied mallei in which the center of mass is displaced from the middle ear suspension points. This feature will be shown to enhance low-frequency inertial bone conduction.

The objectives of this investigation were to study the ossicular motion in *Chrysochloris asiatica* in response to vertical and horizontal substrate vibrations.

Materials and methods

Animals

This study was based on data from seven adult Cape golden moles (*Chrysochloris asiatica* L.), four females and three males, caught in Cape Town (South Africa) and kept in captivity at the University of Cape Town (UCT) for at least two weeks before shipment to the University of California, Los Angeles, USA (UCLA). While in captivity they were kept in plastic containers (0.6×0.4 m) filled with approximately 15 cm of moist soil at room temperature (15–25°C) and provided with mealworms (*Tenebrio* sp. larvae) and diced lamb kidney daily. The animals were shipped in a specially constructed plastic crate with internal partitions (containing ~10 cm of soil) to house the moles individually; each animal was supplied with mealworms for sustenance. The capture, housing and shipping of the animals was sanctioned by the UCT Science Faculty Animal Experimentation Committee (AEC#2004/V3/GNB). Once at UCLA, the animals were kept in captivity for at least five days prior to the initiation of the experiments. Since golden moles have internal sexual organs and do not exhibit any visible sexual dimorphism, their gender was determined in a *post-mortem* examination.

Two animals were used in control experiments, while the dynamic behavior of the ossicular chain in response to seismic stimuli was investigated in the remaining five animals. For anatomical measurements, six additional specimens were available that had been subjects in a preliminary experiment. The three-dimensional (3-D) reconstruction of the middle ear was based on one specimen fixed in 94% ethanol.

3-D anatomy

In order to obtain detailed information on the 3-D anatomy of the middle ear, the hearing apparatus (external ear, middle ear and parts of the inner ear) of one specimen was scanned by means of microcomputed tomography (μCT; Scanco Medical Co., Bassersdorf, Switzerland; model μCT20; image matrix, 512×512 pixels; angular increment, 0.36°). The specimen was fixed in 94% ethanol and kept in physiological saline for 24 h prior to the scanning. The skull was trimmed to a minimum size that still included the structures of interest (the semicircular canals were lost). The specimen was scanned using a voxel size of 12 μm on a side. During this ~6 h procedure, the specimen was kept moist in a sealed container. Based on virtual slices, the skull and the ossicluar chain were separately rendered in three dimensions.

Preparation

Animals were euthanized with an overdose of isoflurane (Abbott Labs, N. Chicago, IL, USA). The bottom of a cylindrical, transparent air-tight container (diameter, 0.14 m; height, 0.15 m) was one-third filled with topsoil. A piece of isoflurane-saturated (2–3 ml) gauze was placed on top of the soil, and the container was sealed. Evaporation during 2–3 min at room temperature resulted in an isoflurane concentration of 30–35% in air. The animal was then placed in the container, which was then resealed. After 5 min, the animal was removed from the container. Prior to any surgical intervention, an additional 5 min elapsed. During that time, head dimensions, body mass and body length were measured. If the heartbeat was absent at the end of this period, the surgical preparation was initiated. If a heartbeat was still evident, the animal was again placed in the isoflurane container for 5 min, or until all signs of life had ceased, and then prepared for surgery.

The skull was separated from the body and the skin, and most soft tissues were removed from the skull (Fig. 1A). A frontal section parallel (±10°) to the plane described by the long axes of the two mallei divided the skull into two parts (Fig. 1B); the dorsal part was mounted on a stainless steel disc (diameter, 38 mm; thickness, 3.2 mm) with acrylic resin (Duralay, Reliance Dental Manufacturing Co., Worth, IL, USA) (Fig. 1C). After curing (~5 min), both middle ears were accessed through the posterior openings in the skull. In order to reach the base of the skull, approximately one-third of the brain was removed on each side. The malleus then became visible through the translucent bony shell (base of the skull), which separates the middle ear cavity from the brain. In order to access the distal half of the malleus head from the posterior side, parts of this shell were removed. The bony wall that terminates the middle ear cavity laterally was also partly removed, allowing lateral and posterior exposure of the malleus for the laser Doppler measurements. For a photograph of this preparation, with the measurement grid superimposed on the malleus head, the reader is referred to fig. 5 in Willi et al. (in press).

The stainless steel disc was then inserted into the circular impression in an aluminum block (44×44×13 mm). One screw at each corner of the block tightly affixed the disk to the block. Loosening the screws and turning the disc enabled alignment of the skull relative to the laser beam.

Desiccation of the middle ear structures was minimized by opening the middle ear cavities as little as possible and by
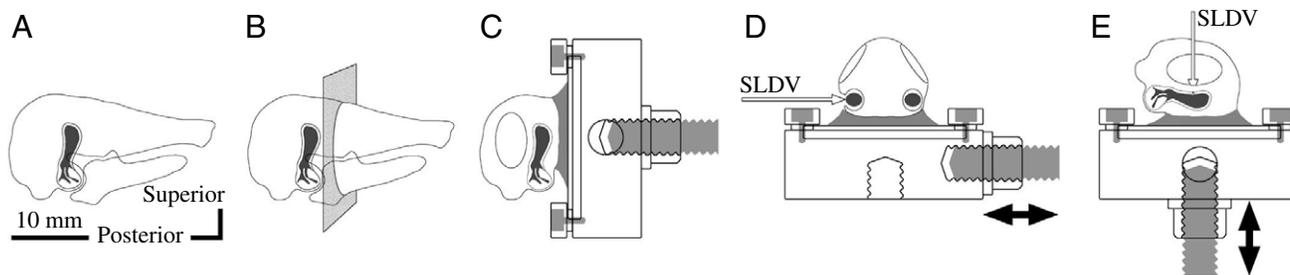
Fig. 1. (A) Lateral view of skull (*C. asiatica*). The dimensions in the sketch are to scale and illustrate the enormous relative size of the hypertrophied malleus (black shading) as well as its position and orientation within the skull. (B) In order to attain optimal coupling between the skull and the vibration exciter, the skull was divided into two sections by a frontal plane cut and (C) the posterior half was mounted on a stainless steel disc with acrylic resin. The disc was secured to a mounting block, which could be driven by a vibration exciter. Seismic stimuli were applied in two different directions. (D) For lateral stimuli, the malleus heads were within the horizontal plane and the excitation was coplanar but perpendicular to the long axes of the mallei. (E) For vertical stimuli, the skull remained in place but the excitation direction was changed.

moisturizing the surrounding tissue, the skull and the middle ear cavities between the experiments.

Seismic stimulation

For lateral skull stimulation, the mallei were horizontally aligned (Fig. 1D). In a second experiment, the aluminum block and the skull maintained their relative orientation, but the vibration exciter (4809; Brüel & Kjaer, Nærum, Denmark) was now attached to the bottom of the aluminum block in order to vibrate it vertically (Fig. 1E).

Signal generation and data acquisition were both software controlled (PSV 7.4; Polytec, Waldbronn, Germany). A periodic chirp sweeping from 10 to 600 Hz (duration, 1 s; frequency resolution, 1 Hz) was generated by the built-in signal generation board (NI 6711; National Instruments, Austin, TX, USA). The stimulus amplitude was adjusted by a stereo amplifier (NAD, 3020A; Boston, MA, USA) placed between the signal generation board and the vibration exciter.

Prior to each experiment, the signal was calibrated in order to attain a flat velocity response (1×10^{-4} m s^{-1}) at the skull along the axis of excitation. This was done by first measuring skull velocity as a function of stimulus frequency, which reflected the characteristics of the vibration exciter with its load. Then, this file was inverted, creating a compensation file, which was multiplied by the original driving file. The output of this multiplication was the file applied to the vibration exciter for driving the skull. The resulting skull motion deviated by a maximum of 1 dB from the desired velocity amplitude (1×10^{-4} m s^{-1}).

Velocity measurements

In order to describe the complete ossicular response, velocities of the malleus, incus and stapes must be obtained. As will be shown, the incus and the malleus move as one functional unit and, therefore, only the dynamic response of two ossicles needs to be monitored: the stapes and the incudo-mallear complex. Unfortunately, the stapes is deeply embedded in the skull, providing either limited or no access. Velocity measurements were therefore restricted to the

peripheral part of the malleus head, which required minimal opening of the middle ear cavity.

The ossicular motion was monitored by means of scanning laser Doppler vibrometry (SLDV). This system (PSV-300; Polytec) performs automated velocity measurements at multiple points on a grid covering a defined area at a user-defined spatial resolution. The built-in video camera (FCB-IX47P; Sony, Minokamo, Japan), which is optically in line with the laser beam, is equipped with optical zooming and enables screen-controlled section and grid selection and positioning of the laser beam. Prior to each scan, a video image of the object to be measured was captured and stored. Alignment of the SLDV relative to the specimen was facilitated by a two-dimensional *XY*-translation stage (Newport, Irvine, CA, USA) and a telescopic lifting column (TGC 8AWD3; Magnetic, Liestal, Switzerland), respectively.

During velocity measurements in response to both lateral and vertical stimulation, the laser beam was in line with the excitation direction. For vertical measurements, the laser head's horizontal position was maintained but the laser beam was deflected downwards by 90° using a first-surface mirror (Rolyn-Optics, Covina, CA, USA) placed at an angle of 45°. The mirror was rigidly attached to the laser head by a solid aluminum extension arm. At the distal end of the extension arm, an accelerometer (4370; Brüel & Kjaer) monitored any induced SLDV motion. This motion was minimized by mechanically separating the vibration exciter from the table surface using an open-cell foam mat (25 mm) and a rubber mat (6 mm). The effect of ambient seismic disturbances was attenuated further by mounting the entire setup on a massive table top (RS-4000; Newport) supported by high-performance laminar flow isolator legs (I-2000; Newport, Irvine). The setup for vertical stimulation is illustrated in Fig. 2.

The scan of one ear comprised 20–40 points on a measurement grid that covered the distal portion of the malleus head and parts of the skull for reference purposes. For SLDV measurements of the malleus from the posterior side in response to vertical stimulation, both mallei were in the field of view and, by defining two separate measurement grids, both
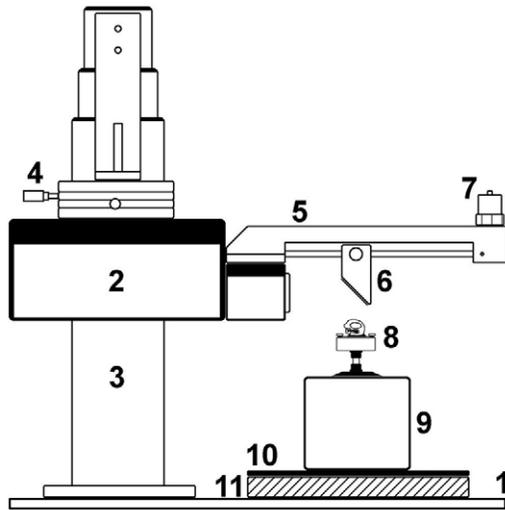
all other points. Next, the velocity of the skull reference point was subtracted from all points.

The motion of a rigid object measured from a single side by means of the SLDV can be decomposed into three motion components: one translation in line with the laser beam and two rotations in which both rotational axes reside in a plane perpendicular to the laser beam. The three motion components are defined by applying the rigid body motion equation:

$$\vec{v} = \vec{v}t + \vec{\omega} \cdot \vec{r} = \begin{bmatrix} v_x = v_x t + (\omega_y \cdot r_z - \omega_z \cdot r_y) \\ v_y = v_y t + (\omega_z \cdot r_x - \omega_x \cdot r_z) \\ v_z = v_z t + (\omega_x \cdot r_y - \omega_y \cdot r_x) \end{bmatrix} . \quad (1)$$

The equation describes the 3-D motion of a rigid body, where r_x, r_y and r_z are distances from the origin of the reference frame (coordinate system) and $v_x t$, $v_y t$, $v_z t$, ω_x, ω_y and ω_z are the six possible velocity components. For lateral stimulation, for example, only the coordinates r_x, r_y were available, and the velocity components $v_z t$, ω_x and ω_y could be calculated. Equation 1 is thereby reduced to:

$$v_z = v_z t + (\omega_x \cdot r_y - \omega_y \cdot r_x) . \quad (2)$$

In order to achieve comparable results from the three velocity components, the measurement coordinate system was aligned to particular anatomical landmarks. The tip of the short process of the incus (SPI) served as the origin of the measurement coordinate system for vertical and lateral measurements since it appears to be the firmest attachment between the ossicular chain and the skull. The x-axis is the long axis of the malleus whereas the z- and y-axes are in line with the SLDV measurement for lateral and vertical stimulation, respectively. Fig. 3A illustrates the alignment of the three-dimensional coordinate system.

SLDV measurements of the distal portion of the malleus head reveal the velocity modes and resonant frequencies of this ossicle but give no direct information about the dynamic behavior of the stapes, which drives the oval window – the input to the inner ear. In order to determine the ossicular motion near the stapes, the motion at the lenticular process of the incus (LPI) was calculated based on the velocities of the malleus head. First, the three velocity components were calculated and, second, the rotational velocities were multiplied by the corresponding coordinates of the LPI. Translational velocities are constant for all measurement points. For lateral stimulation, we calculated the resultant of all three motion components at the LPI using Eqn 2. For the LPI-motion reconstruction, two position coordinates (r_x, r_y) and the three motion components (ω_x, ω_y, $v_z t$) were the known variables, and v_z was calculated.

The coordinates of the LPI were obtained after the experiment by carefully removing the structures that masked the proximal parts of the ossicular chain during the experiment. The skull was then accurately realigned (±0.1 mm in the x- and y-directions) relative to the video camera image, in order to present the same view as during the measurement. This picture

Fig. 2. Setup for vertical excitation. The entire setup is placed on a high-performance laminar-flow isolation table (1). The scanning laser Doppler vibrometer (SLDV) (2) is suspended and positioned in three dimensions by a telescopic lifting column (3) and a *XY*-translation stage (4). A solid extension arm (5), only used during vertical excitation, allowed positioning of the first-surface mirror (6), tilted at an angle of 45° in order to deflect the laser beam downwards by 90°. At the distal end of the extension arm, an accelerometer (7) monitored the motion of the arm during the experiment. The specimen was tightly mounted to a metal block (8), which was driven by the vibration exciter (9). In order to avoid transmission of vibrations to the SLDV *via* the supporting table, a rubber mat (10) on top of an open-cell foam mat (11) separated the table from the vibration exciter.

ears could be measured without changing the head position. By contrast, for malleus measurements with lateral stimulation, only one ear was in view at a time.

Data acquisition occurred at a frequency resolution of 1 Hz, and both the amplitude and phase of the measured velocities were averaged five times for each point on the measurement grid. Data from the accelerometer and the SLDV were acquired in parallel. Once a measurement was completed, all data points could be animated at a discrete frequency and, by linking the picture captured by the video camera to the measurement grid, the dynamic response of the measured structure could be viewed.

Data processing and analysis

The goal of this study was to quantitatively describe the middle ear dynamics for two different seismic stimulation directions in order to estimate the effective stimulus for the inner ear in the two cases. To do that, the ossicular motion relative to the skull was calculated by subtracting the skull velocity from the malleus velocity. The signal generator was used as an external phase reference for all measurement points. As a first step in the analysis, a reference point on the skull was defined among the measurement points, and its phase was subtracted from all measurement points. In this way, the phase of this point became zero and served as a phase reference for

was superimposed on the picture captured prior to the measurement, and the coordinates of the LPI and the SPI were evaluated based on the coordinate system of the measurement grid.

Predictions about the dynamic behavior of a structure outside the observable area are only justified if both the area being measured and the structure outside the observable area are part of the same rigid body. In a preliminary control experiment, the ossicular chain was widely exposed from the SPI to the distal end of the malleus by accessing the middle ear cavity posteriorly. The ossicular response to a vertical stimulus (frequency band, 10–600 Hz; skull velocity, 1×10^{-4} m s^{-1}) was obtained at a high spatial resolution (~0.4 mm). Measurement points lying on a straight line crossing the incudo-mallear joint (IMJ) were selected for analysis. The real part of the velocity was plotted against the imaginary part of the velocity for each measured point for three frequencies (150, 350 and 545 Hz). If the points fall on a straight line in such a plot, the malleus and incus are dynamically functioning as one unit (Schön and Müller, 1999).

LPI motion reconstruction in response to lateral stimuli was calculated from Eqn 2 using all three motion components (ω_x, ω_y and v_zt). Since the LPI and the SPI both reside in the measurement (x–y) plane, all three components act in the same medio-lateral direction at the LPI (Fig. 3B). This is not the case for LPI motion reconstructions in response to vertical stimuli, since the LPI and the SPI do not both reside in the measurement (x–z) plane. At the LPI, the ω_x-component acts in the medio-lateral, the ω_z-component in the infero-superior and the v_yt-component in the antero-posterior direction (Fig. 3C). Since these three motion components are not in line but are oriented perpendicular to each other, three separate LPI motions (LPI$_x$, LPI$_y$ and LPI$_z$) were calculated applying Eqn 2.

Results
Control experiments

To quantify the stimulus-induced vibrations reaching the SLDV, the skull was driven vertically while simultaneous measurements were made of (1) the skull velocity (with the SLDV) and (2) the extension arm and, therefore, the SLDV motion (with the accelerometer). A baseline measurement was performed in the absence of a driving signal. In a second measurement, a compensated driving signal was applied, which resulted in a flat skull velocity response of 1×10^{-4} m s^{-1} (±0.5 dB) over the frequency range tested. Fig. 4A shows this SLDV measurement (constant vertical skull velocity) as well
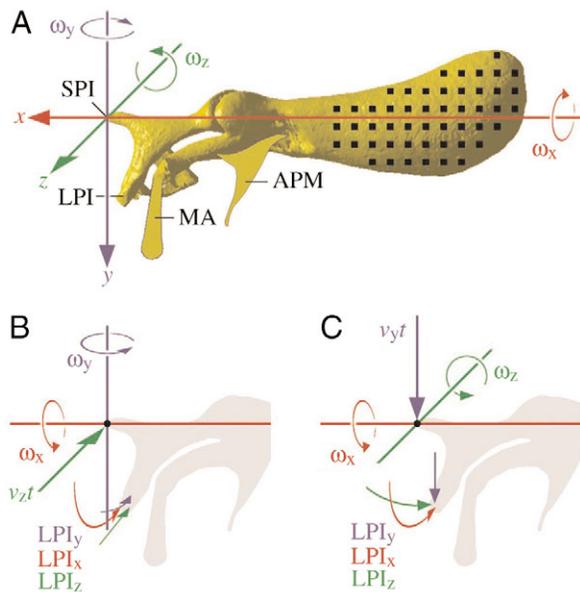

Fig. 3. (A) Lateral view of the ossicular chain of *C. asiatica* obtained by microcomputed tomography (μCT). The coordinate system for the measurement points (black squares) was aligned to anatomical landmarks. The *x*-, *y*- and *z*-axes and the rotations about them (ω_x, ω_y and ω_z) describe the six possible degrees of freedom of the ossicular chain. The anterior process of the malleus (APM) and the manubrium (MA) were added manually and were not rendered in 3-D from the μCT data set. (B) Reconstruction of lenticular process of incus (LPI) motion based on three motion components for lateral and (C) vertical stimulation. The indicated motion directions (ω_x, ω_y, ω_z, v_yt and v_zt) in B and C are adjusted in order to point towards the LPI, whereas in A they indicate the mathematically correct polarity of the vectors. SPI, short process of incus.
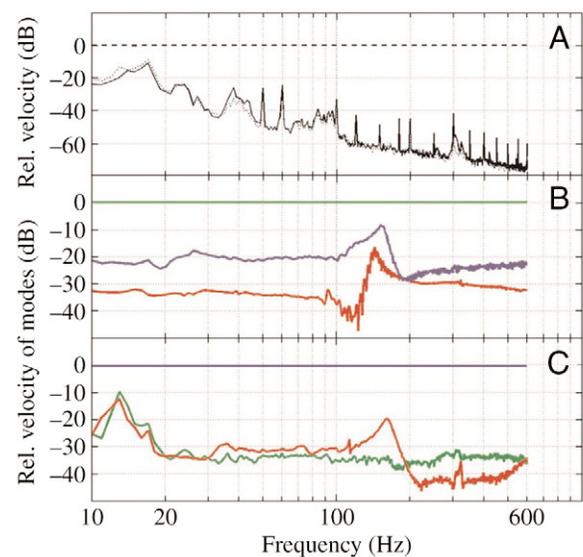

Fig. 4. Two control experiments. (A) Verification of induced vibrations on the scanning laser Doppler vibrometer (SLDV) and the extension arm. The noise level was measured with the accelerometer at the tip of the extension arm (dotted line). During application of a vertical stimulus (frequency, 10–600 Hz, velocity, 1×10^{-4} m s^{-1}), the skull velocity was measured with the SLDV (dashed line) while the accelerometer simultaneously monitored the motion of the extension arm (solid line). (B) Relative plot of the mounting block response in three orthogonal directions for lateral and (C) vertical stimulation. The colors refer to those in Fig. 3A. The driving direction (intended excitation direction) of the vibration exciter is represented by a flat line at 0 dB (green line for lateral, and blue line for vertical stimulation, respectively).

as the accelerometer measurements with and without the applied driving signal. The two accelerometer measurements are very similar and, moreover, the driver-induced SLDV vibrations are negligibly small compared with the skull motion measured under the experimental conditions. Except for frequencies below 20 Hz, the signal-to-noise ratio (SNR) is at least 25 dB. Due to the rather small SNR below 20 Hz, results in this range must be interpreted with caution. This control experiment clearly demonstrates that for frequencies above 20 Hz, no significant portion of the vibration emitted by the vibration exciter reaches either the SLDV or the mirror mounted on the extension arm.

A second control experiment concerned the effective stimulus applied to the skull. In principle, a vibration exciter has a single defined excitation axis, but in practice, especially at higher frequencies and under asymmetric load conditions, complex motion modes can occur. To detect possible transverse modes, the motion of the specimen block was measured from three orthogonal directions for both vertical and lateral excitations. The measurement directions and the colors used to display the results in Fig. 4B,C follow the coordinate system depicted in Fig. 3A. The response of the indicated mode is in line with the corresponding axis. The 0-reference lines in the two graphs represent the response in the desired stimulation direction, whereas the other two responses represent transverse modes that are oriented perpendicular to the stimulation direction. The results show the presence of side mode peaks between 120 and 160 Hz. For lateral stimulation, a vertical mode is induced with a peak amplitude ~10 dB below that along the driven axis. For vertical stimulation, the peak amplitudes of these side modes are at least 20 dB below the amplitude generated along the driving direction. Repetitive measurements under modified conditions (shaker orientation was changed, the length of the holder mounting screw was varied and the holder was loaded with different masses) revealed that the resonant frequencies and peak amplitudes of these side modes are very stable, and thus we conclude that they are intrinsic to the vibration exciter. These modes are therefore unavoidably present during the measurements, are not suppressed and must be considered when interpreting the results.

In a third control experiment we tested the hypothesis that the malleus and incus function as one dynamic unit within the frequency band tested (10–600 Hz). The velocities of all measured points that lay on a line extending from the SPI to the distal end of the malleus head are plotted in Fig. 5 as their real *vs* imaginary parts in response to three frequencies (150, 350 and 545 Hz). Velocity measurements of three points on the incus (open circles) and 12 points on the malleus were obtained at each frequency. The results show that points falling on a straight line along the ossicular chain exhibit complex velocity parameters that describe a reasonably straight line in real–imaginary space (Fig. 5). This condition is only fulfilled by a functionally rigid body. Since this condition holds across the incudo-mallear joint, the rigid-body assumption, and thus our LPI-motion reconstruction procedure, is justified.
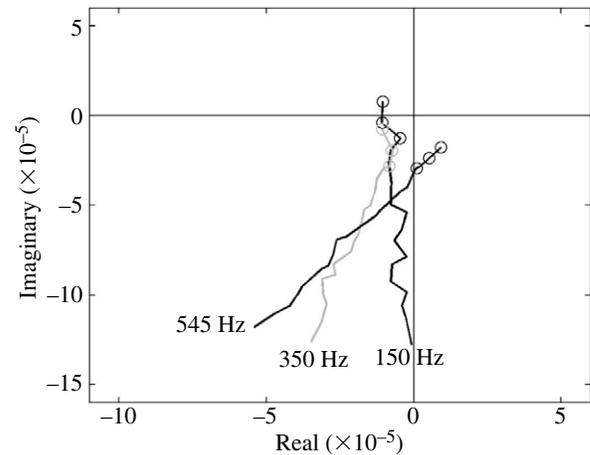

Fig. 5. Velocities measured at 15 points on a line along the ossicular chain are plotted in the Gaussian plane (real–imaginary). The real and the imaginary parts of the velocity measured from the 15 points; three on the incus (open circles) and 12 on the malleus, are plotted for three different frequencies (150, 350 and 545 Hz). The points on both malleus and incus represent a reasonably straight line, which indicates that the measured points are located on structures (malleus and incus) that dynamically function as one unit.

3-D anatomy

Based on μCT, the ossicular chain of one specimen was rendered in three dimensions as depicted in Fig. 6 in lateral, anterior, medial and posterior views (from top to bottom). The relative orientation of the ossicles within the skull and the axis orientation relative to the ossicles can be seen in Fig. 1A and in Fig. 3A, respectively. The manubrium (MA) and the anterior process of the malleus (APM) were resolved automatically by μCT but were lost during the 3-D-rendering process and therefore were manually supplemented, based on dissected material. Fig. 7 depicts two original μCT-reconstructed virtual sections, showing the relative sizes of the middle ear structures in *C. asiatica*.

From the SPI to the superior end of the malleus head, the ossicular chain spans a distance of 7.6±0.2 mm (mean ± s.d.; *n*=20 measurements). *C. asiatica* has a mean body mass of 42±5.0 g (*n*=13), whereas the three ossicles have a combined dry mass of 22±0.3 mg (*n*=18). Although 80% of the malleus head is composed of dense bone, the content of the residual internal space is unknown. The malleus in this species exhibits a slightly curved, club-like shape with the concave side facing the base of the skull (Fig. 1A). The long axis of the malleus resides in an inferior–superior line with the body of the incus and the SPI, whereas the long process of the incus and the MA project anterior-inferiorly. The malleus and incus are connected by the IMJ. Mechanical probing of the malleus or incus with a needle revealed that the joint yields readily to statically applied forces. Separation of the IMJ is straightforward, revealing two smooth surfaces held together by a ligament encapsulating the entire joint.

The four views of the ossicular chain (Fig. 6) show that the axis perpendicular to the stapes footplate is not in line with the
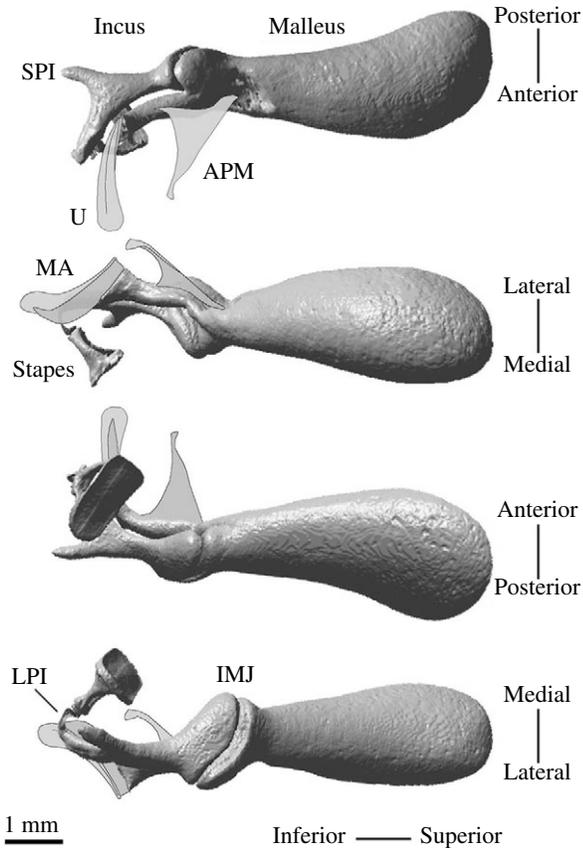
Fig. 6. Four views of the ossicular chain of *C. asiatica* derived from the three-dimensional data obtained by means of microcomputed tomography (μCT). The manubrium (MA) and the anterior process of the malleus (APM) were lost in the 3-D rendering process and were manually inserted. IMJ, incudo-mallear joint; LPI, lenticular process of the incus; SPI, short process of the incus; U, umbo.
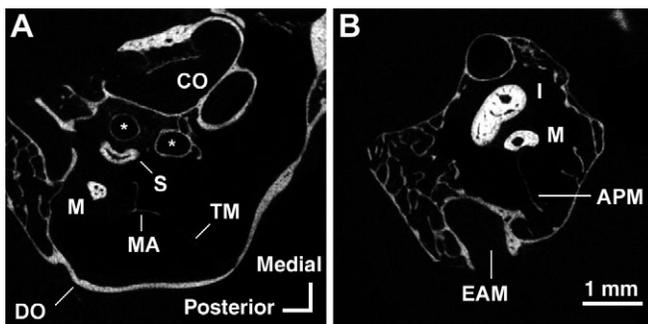

Fig. 7. Two examples of original μCT-reconstructed cross sections through one middle ear of *C. asiatica*. The sections are therefore in parallel and 1.8 mm apart. (A) Cross-section through the tympanic membrane (TM) and the manubrium (MA). (B) Cross section 1.8 mm towards the tip of the malleus (M) head, showing the thin structure of the anterior process of the malleus (APM). The asterisks represent the stapedial artery (it bifurcates before it passes the stapes and fuses again after it passes it). I, incus; S, stapes; CO, cochlea; EAM, external auditory meatus; DO, dome (bony shell of external auditory canal near the TM).

medio-lateral axis but rather points in a postero-medio-superior direction. Morphometric examination in five ears revealed that this axis intersects both the sagittal (x–y) plane and the frontal (x–z) plane at a minimal angle of 44±5.5° and 50±3.4°, respectively.

The ossicular chain is suspended by the tympanic membrane (TM), the APM, the ligament of the SPI and the annular ligament surrounding the stapes footplate. The only middle ear muscle present in *C. asiatica* is the m. stapedius, which connects the posterior crus of the stapes to the skull *via* the stapedial ligament, but the ear lacks the m. tensor tympani and its ligament, as in other golden moles (Von Mayer et al., 1995; Mason, 2003a).

As mentioned above, the APM and the MA were lost by the rendering process due to their very thin structure. From the 2-D slices sampled by μCT taken at a spatial resolution of 12 μm, it was concluded that the thickness of these structures is in the range of 10–80 μm. The tip of the APM is firmly attached to the skull close to the periphery of the TM, yet the APM itself is very flexible when moist and it projects like a curved tapering sheet from the malleus towards its lateral tip over a length of 1.1±0.2 mm (*n*=5). The APM intersects the sagittal plane at an angle of 42±4° (*n*=5).

In profile (cross-section perpendicular to the TM and to the long axis of the MA) the MA resembles a T-bar, the horizontal element being in contact with the TM, the vertical element building the medial connection to the solid neck of the malleus. The vertical element of the T-bar is present along the entire length of the MA, and therefore the connection between the TM and malleus constitutes a very fine osseous structure (Fig. 6, second panel from top).

A third remarkably fine structure is the LPI, which builds an interface between the incudo-stapedial joint and the long process of the incus. The posterior view illustrated in the bottom panel of Fig. 6 shows the thin, slightly curved process that emerges from the distal end of the long process of the incus and reaches the incudo-stapedial joint at its infero-anterior edge. Compared with the fragility of the LPI, the incudo-stapedial joint itself appears to couple the two ossicles in a solid manner and it is very likely that the LPI yields more to an applied force than would the incudo-stapedial joint (Funnell et al., 2005).

Among 15 stapes examined, the following common characteristics were found. The two crura and the stapes footplate form a nearly circular passage through which the stapedial artery passes. The anterior crus forms an arch whereas the posterior crus projects in an almost straight line towards the stapes footplate. At the lateral end of the posterior crus, the stapedial tendon attaches to the stapes, from where it reaches the skull in an infero-posterior direction. With a length of 1.98±0.06 mm and a width of 1.06±0.06 mm, the stapes exhibits a relatively large footplate area (2.1±0.17 mm^2) but is only 1.12±0.13 mm high. The thickness of the stapes footplate rim, to which the annular ligament attaches, is not constant. The rim of the stapes footplate is thick and rounded posteriorly whereas it is very thin and oblate anteriorly. Visual
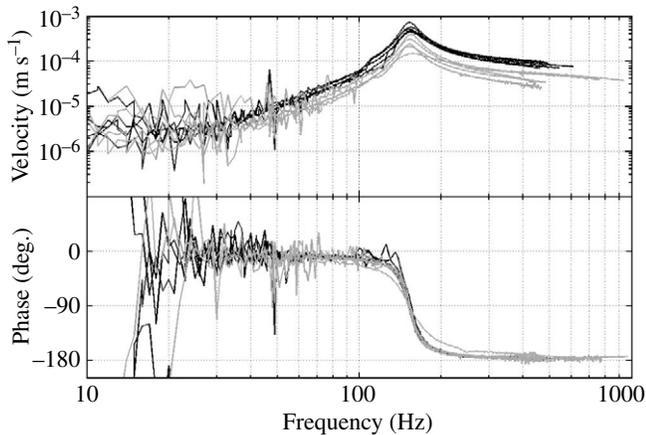
Fig. 8. Relative ossicular response at the distal tip on the malleus head in line with the stimulation direction of the same five right ears for lateral (black) and vertical (gray) stimulation. Each frequency response was shifted along the logarithmic frequency scale to bring the resonant frequencies into alignment at an arbitrary frequency of 150 Hz. Over the frequency band tested, malleus velocity amplitudes in response to lateral stimulation exceeded those in response to vertical stimulation.

Table 1. *P-values from a univariate analysis of variance (ANOVA) comprising the data of 10 ears (the left and the right ears of five specimens)*

Dependent variable	Factor	*P*-value
Resonant frequency	Side	0.687
	Stimulus direction	0.687
Q_{3dB}	Side	0.852
	Stimulus direction	0.275
Peak amplitude	Side	0.237
	Stimulus direction	<0.001

The variables 'resonant frequency', 'Q_{3dB}' and 'peak amplitude' were tested for possible dependence on the factors 'side' and 'stimulus direction'.

examination of the annular ligament revealed that its width also varies significantly between the anterior and posterior aspect of the footplate. At the posterior side, the ligament spans a small gap between the footplate and the skull, whereas anteriorly it overlaps with the rim area of the footplate and the skull, which results in the ligament being wider on the anterior than on the posterior side.

Dynamic behavior

The relative motion of a point within 1 mm of the distal tip of the malleus head is shown for lateral and for vertical stimulation for five right ears in Fig. 8. Statistical analysis was performed on the single point measurements at the periphery of the malleus head in 10 ears (the right and left ears of five specimens). The advantage of this data set is that it lends itself to a univariate analysis of variance (ANOVA) to test for possible ear-side effects and stimulus type.

The resonant frequencies of the 10 ears measured for both stimulation directions cover a relatively broad frequency band ranging from 71 to 200 Hz (mean ± s.d., 135.7±49 Hz) but, for the sake of clarity, the responses of the five right ears shown in Fig. 8 were shifted along the logarithmic frequency axis to align the resonant frequencies at an arbitrary frequency of 150 Hz. Below resonance, the malleus and the skull are in phase, whereas above resonance the skull and malleus motions are 180° out of phase. Three variables were obtained for each frequency response of the 10 ears: the original resonant frequency, the peak velocity amplitude and the sharpness of tuning of the resonance (Q_{3dB}). Each of these variables obtained for lateral stimulation was compared with those obtained for vertical stimulation, and variables obtained from right ears were compared with those obtained

from left ears; the *P*-values for all statistical tests are listed in Table 1.

The differences in distribution of the three dependent variables are not accounted for by the factor 'side of the ear'. Moreover, the stimulus direction does not explain the difference in resonant frequency or Q_{3dB} value. However, lateral stimulation results in a mean peak amplitude at the malleus' distal end that is 5.8±2.8 dB greater than that for vertical stimulation. In fact, over frequencies between ~50 and 600 Hz, the ossicular velocity induced by lateral stimulation consistently exceeds that induced by vertical stimulation (Fig. 8).

Motion decomposition

In a second step, the malleus motion was decomposed into three motion components: one translation and an *x*- and a *y*-rotation for lateral stimulation, and one translation and an *x*- and a *z*-rotation for vertical stimulation. These three components can be used to calculate the velocity amplitude at any point of the coordinate system. To visualize the ossicular motion pattern, velocity amplitudes were calculated for a grid generously covering the ossicular chain at a spatial resolution of 0.5 mm along both axes involved (*x* and *y*, or *x* and *z*). The relative velocity amplitudes were color coded, blue and red representing low and high values, respectively, and are shown as iso-amplitude lines for lateral (Fig. 9A) and vertical (Fig. 9B) stimulation. For both stimulation directions, the ossicular chain oscillated about the tip of the SPI in all specimens tested.

Calculation of the *z*-component of the LPI motion under lateral stimulation yields the same result when Eqn 2 is applied, independent of the orientation and position of the coordinate system. This is the case since all three components (ω_x, ω_y and $v_z t$) induce coaxial motion at the LPI (Fig. 3B). By contrast, when vertically stimulated, the three components (ω_x, ω_z and $v_y t$) act in different directions at the LPI (Fig. 3C) and must be calculated separately. Therefore, it is essential to align the coordinate system with the motion pattern in order to make meaningful amplitude comparisons between the three components at the LPI (LPI$_x$, LPI$_y$, LPI$_z$). The angle between
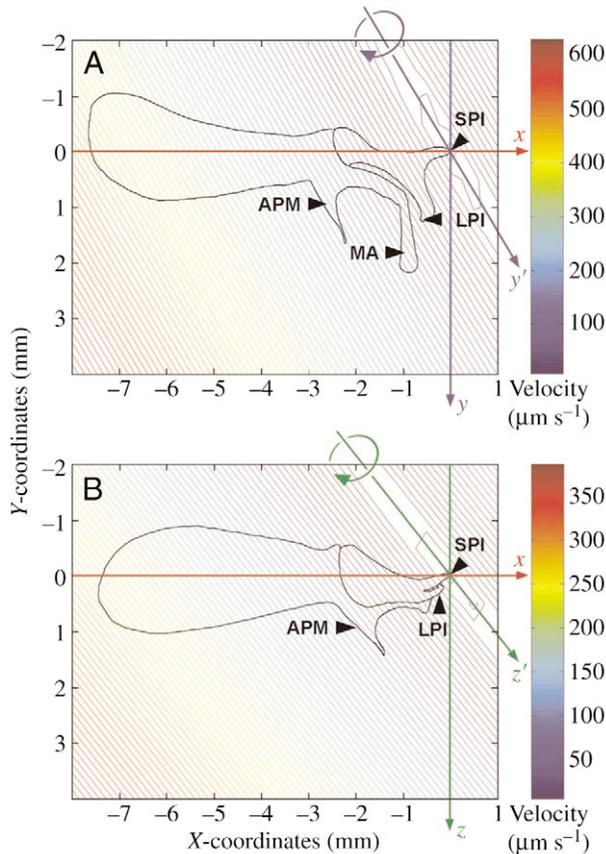
Fig. 9. Iso-velocity amplitude map for lateral (A) and vertical (B) stimulation based on the SLDV measurements of the malleus head. The two graphs represent the motion pattern at the resonant frequencies 178 Hz and 182 Hz, respectively, measured from the left ear of animal #17. Velocity amplitudes were calculated by applying Eqn 2 at each point of a grid at a spatial resolution of 0.5 mm. The map and an outline of the ossicular chain are superimposed to indicate the motion pattern with respect to the ossicular anatomy. The axes of minimal amplitude are indicated by the y'- and z'-axis, respectively. For the LPI-motion reconstruction in response to vertical stimulation, the coordinate system was aligned with respect to the z'-axis. APM, anterior process of malleus; LPI, lenticular process of the incus; MA, manubrium; SPI, short process of the incus.

Fig. 10. (A) For lateral stimulation, the LPI motion in the medio-lateral direction was reconstructed based on the three motion components: ω_x, ω_y and $v_z t$, and the results are given for the same five right ears whose response is depicted in Fig. 8. Upper graph, amplitude responses; lower graph, phase responses. (B) For vertical stimulation, the LPI motion was reconstructed separately for the three motion components $\omega_{x'}$, $\omega_{z'}$ and $v_y t$, resulting in the three orthogonally oriented LPI motion components $LPI_{x'}$, $LPI_{z'}$ and LPI_y. Consistent and reproducible results were observed only for the $\omega_{z'}$-component ($LPI_{z'}$).

the z- and the z'-axis was measured for each experiment, and the coordinate system rotated so that the z'-axis represented the new z-axis (Fig. 9B). The plots of total relative (with respect to the skull) LPI motion of the right ears of five specimens are shown for lateral stimulation (Fig. 10A), and the three LPI motions (LPI_x, LPI_y, LPI_z) separately derived from the three motion components (ω_x, ω_z and $v_y t$) are shown for vertical stimulation (Fig. 10B). At resonance, in response to lateral stimulation, the mean velocity amplitude reached $1.83\pm0.19\times10^{-4}$ m s^{-1} ($n=10$) and thereby exceeded that at which the skull vibrates (1×10^{-4} m s^{-1}) by 5.2 ± 0.9 dB. The LPI motions for the same five ears whose responses are shown in Fig. 10A are shown in Fig. 10B separately for $LPI_{x'}$, $LPI_{z'}$ and $LPI_{y'}$ in response to vertical stimulation. In all five right
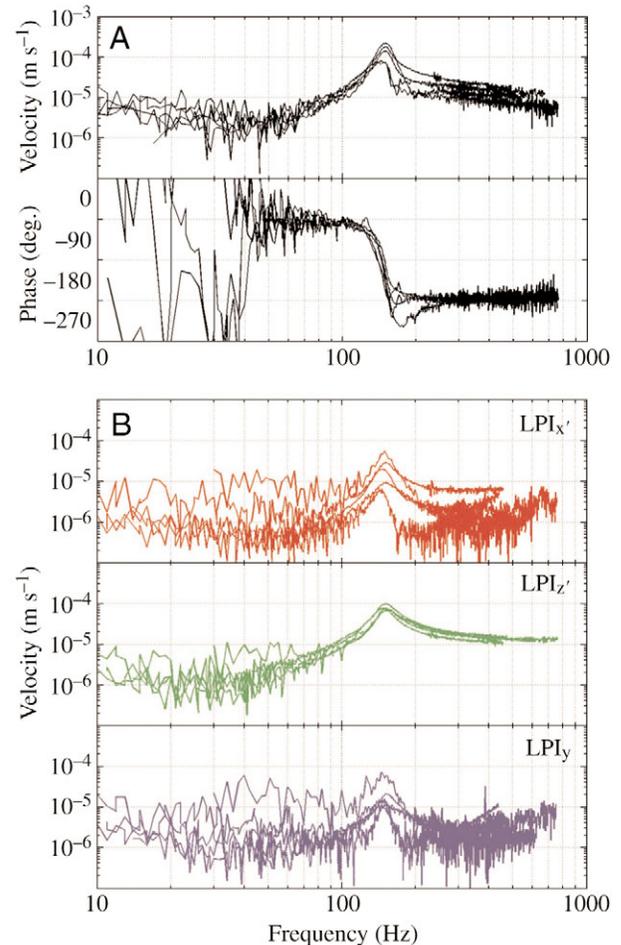
ears tested, the LPI motion induced by the z'-rotation dominated the other two contributions. At resonance, the mean z'-contribution equals $0.80\pm0.12\times10^{-4}$ m s^{-1}, the mean x'-contribution $0.27\pm0.24\times10^{-4}$ m s^{-1} and the mean translational contribution $0.28\pm0.30\times10^{-4}$ m s^{-1}. Fig. 10B also illustrates that the LPI motion induced by the z'-rotation is the most consistent among all five specimens and shows a smoother course compared with the other two components.

Discussion

Anatomy

Within the Chrysochloridae, a great variety of middle ear phenotypes can be found (Broom, 1927; Cooper, 1928; Hyrtl,

1845; Mason, 2003a). While two genera (*Amblysomus* and *Neamblysomus*) have a 'typical' mammalian malleus, others have developed a ball-shaped (*Eremitalpa, Chrysospalax)* or club-shaped (*Chrysochloris, Cryptochloris)* hypertrophied malleus, and species of *Chlorotalpa* exhibit intermediate morphological variations. It has been suggested that the hypertrophied malleus enables the detection of seismic disturbances (Fielden, 1991; Mason, 2003b; Narins et al., 1997). The underlying mechanism implicated in this detection is inertial bone conduction, which requires a middle ear mass that vibrates less than the skull due to its inertia and thereby generates relative motion between the stapes footplate and the skull. At low frequencies, a mechanical system such as the mammalian middle ear rotates principally about an axis defined by the ligaments – the suspension of the ossicular chain within the middle ear cavity – since the impedance at low-frequency modes is stiffness controlled. The center of mass in a mammalian middle ear with a 'normal' malleus resides along or close to this rotation axis, whereas in chrysochlorids with a hypertrophied malleus the center of mass is displaced from the potential rotation axis defined between two suspension points. This middle ear type exploits the lever effect of the shifted mass.

Since seismic vibrations are only efficiently transmitted at low frequencies (<500 Hz) (Aicher and Tautz, 1990; Brownell, 2001; Hill and Shadley, 2001; Von Dohlen, 1981), an optimal seismic sensor should exhibit little stiffness in order to reduce impedance at low frequencies. Structures in the middle ear of *C. asiatica* in which stiffness is clearly minimized are the APM and the MA. These structures are extremely thin and flexible, and for neither lateral nor vertical seismic stimuli does the APM or the MA represent an anchorage point of the motion modes described in Fig. 9. Both modes represent the motion pattern at the first resonant frequency and are, therefore, 'first modes'.

The APM is acting as a spring as predicted by Mason (2003b). We have observed that if the APM becomes detached from the skull, the malleus inevitably makes contact with the skull wall. To avoid wall contact and the resulting significant sensitivity loss and/or distortion, the malleus must be precisely positioned within the middle ear cavity. This is presumably an important function of the APM – to statically hold the ossicular chain in place.

The T-bar design of the MA reduces the stiffness for modes that involve motion parallel to the TM and perpendicular to the MA. In other words, applying an in-line force to the vertical member of the T-bar results in minimal deformation of the bar, compared with a laterally applied force.

Resonant frequencies

The resonant frequency seen in Fig. 8 is the first resonance described by the relative ossicular motion and is considered to be the first mode. Below that mode the ossicular chain and the skull move in phase and relative motion between them is negligibly small. For most animals, minor differences in resonant frequencies were detected between ears and stimulus types, but these differences are not statistically significant.

In comparison with the relatively small differences in resonant frequency between right and left ears for vertical and lateral stimulation within the same animal, the observed resonant frequency variation between animals (71–200 Hz) is rather high. Variations due to measurement artifacts are possible, but it is likely that natural variation accounts for a significant portion of these intraspecific differences.

Since the animals examined in this study were collected at different places in Cape Town (South Africa) it is possible that these variations are due to adaptations to different soil types. Soil properties such as porosity, density and water content define how well a seismic wave of a certain frequency propagates in the ground (Iida, 1938, 1939; Ishimoto and Iida, 1937). Seismic surface waves are best propagated around 100 Hz (30–300 Hz) in the ground inhabited by the prairie mole cricket (Hill and Shadley, 2001), 300–400 Hz in sand (Brownell, 2001), below 100 Hz in grassy humus (Von Dohlen, 1981) and 300–400 Hz on wet sandy beaches (Aicher and Tautz, 1990).

Interpreting a seismic signal

Locating the source of a seismic disturbance not only implies sensing seismic waves but extracting directional information from them as well. Two questions immediately arise: (1) what directional cues are present in the seismic signals and (2) how does the animal resolve them? Excitation of the middle ear by a seismic disturbance depends on the alignment of the animal's head relative to the ground, the source distance and the waveform reaching the animal. The particle motion around the skull sets the skull in vibration, and the middle ear ossicles respond to the skull vibration.

Several types of seismic waves can be distinguished depending on their position in the substrate and their propagation characteristics. Parameters characterizing a wave are propagation speed, the direction of particle motion and the transported energy (Ewing et al., 1957). Surface waves, i.e. Rayleigh (R)- and Love (L)-waves, propagate only at a boundary between two media (e.g. ground–surface). Body waves (e.g. P-waves) travel within the substrate; they do not require an impedance boundary for their propagation. The particle motion generated by a P-wave is principally along the propagation axis of the wave energy. When P-waves reach a surface, a minor vertical component is generated (Achenbach, 1973). R-waves near the surface generate retrograde elliptical particle motions with a dominant vertical and a smaller longitudinal component. By contrast, particle motion in L-waves occurs in the horizontal plane and is aligned transverse to the direction of propagating wave energy. Attenuation and propagation velocity of these waves depend on the substrate and differ between the three waveforms. Consequently, the temporal pattern and spectral composition of the waveform reaching an animal depend on its distance from the source. Close to the source P-, L- and R-waves are temporally overlapping and interfere with each other but, with increasing distance from the source, they diverge continuously due to their different propagation velocities. P-waves spread

spherically into the ground and attenuate faster ($1/d$) than L- and R-waves, which spread circularly and attenuate as ($1/d^{\frac{1}{2}}$), where d is the distance from the source. Thus, the amplitude, phase and spectral composition of a seismic signal reaching an animal is source-distance dependent (Sommerfeld, 1970).

Determining the class of seismic signals to which an animal is exposed in the field is the subject of future investigations, but it is likely that R-waves are available to the Cape golden mole (*C. asiatica*), as they are to other sympatric fossorial animals (Narins et al., 1992).

The ossicular chain design of *C. asiatica* and our measurements suggest high responsiveness to vibrations in directions orthogonal to the long axis of the malleus, and the present study indicates that both vertical and lateral stimuli have the potential to induce stapes motion. Over the frequency band tested, the ossicular response to vertical stimulation is smaller than the response to lateral stimulation, and at resonance the difference is significant.

The asymmetric shape of the stapes footplate and the variation in annular ligament width suggest an asymmetric stiffness around the footplate. Such an arrangement leads to a rocking stapes motion rather than a piston-like movement in response to ossicular excitation. Considering the alignment of the stapes (Fig. 6) and the motion modes visualized in Fig. 9A,B, both lateral and vertical stimuli drive the head of the stapes sideways (not piston-like), which supports the assumption that rocking is the favored motion mode of the stapes in response to a seismic stimulus. The incudo-stapedial joint firmly connects the two ossicles, but the delicate LPI provides additional degrees of freedom for a stapes footplate rocking motion. The stapes footplate motion induced by lateral or vertical stimulation cannot be quantitatively calculated from the gathered data. However, the fact that the LPI, in response to either stimulation direction, drives the stapes footplate in two distinct rocking motions suggests that the two stimulation directions might be differentiated at the level of the stapes and perhaps in the inner ear.

This study shows that when the mallei are oriented parallel to the ground surface, the ossicular chain could respond to both the vertical- and the horizontal-motion components of the R-wave. The rolling particle motion of the R-wave is retrograde. An R-wave approaching the head from the side would lead to elliptical motion of the mallei if they followed the particle motion of the soil. Since the skull drives the left and right ear simultaneously, the two ossicular chains will respond to this stimulus. Relative to the skull, however, they rotate in opposite directions: if the malleus rotation starts with an upward-inward motion in one ear, the malleus of the other ear undergoes an upward-outward motion. The complex middle ear anatomy could favor a certain rotation direction and, therefore, favor either an ipsi- or a contralaterally approaching R-wave, providing directional information about the source. This hypothesis awaits experimental verification.

The fact that two perpendicularly oriented stimulation directions excite the middle ear to different degrees suggests that the ossicular chain responds more to certain stimulation directions than others. Assuming the animal is in a horizontal posture, so that the mallei are oriented vertically, the longitudinal (horizontal) component of the R-wave reaching the skull from different azimuths would drive the malleus perpendicular to its long axis. If there is a preferred excitation direction, the animal may obtain directional cues. Similar considerations can be made for both middle ear alignments in response to L-waves, which could also provide directional information.

This study leads us to new insights about the perception of directional cues in a fossorial mammal based on an extraordinary middle ear design. Future studies should focus on the seismic environment of *C. asiatica* in its natural habitat and address the question of whether there is indeed a preferred excitation direction that provides the animal with directional information.

References

Achenbach, J. D. (1973). *Wave Propagation in Elastic Solids.* Amsterdam, New York: Elsevier North-Holland.

Aicher, B. and Tautz, J. (1990). Vibration communication in the fiddler crab, *Uca pugilator. J. Comp. Physiol. A* **166**, 345-353.

Barnett, K. E., Cocroft, R. B. and Fleishman, L. J. (1999). Possible communication by substrate vibration in a chameleon. *Copeia* **1999**, 225-228.

Barth, F. G. and Geethabali (1982). Spider vibration receptors; threshold curves of individual slits in the metatarsal lyriform organ. *J. Comp. Physiol. A* **148**, 397-412.

Broom, R. (1927). Some further points on the structure of the mammalian basicranial axis. *Proc. Zool. Soc. (Lond.)* **1927**, 233-244.

Brownell, P. H. (1977). Compressional and surface waves in sand: used by desert scorpions to locate prey. *Science* **197**, 479-482.

Brownell, P. H. and van Hemmen, J. L. (2001). Vibration sensitivity and a computational theory for prey-localizing behavior in sand scorpions. *Am. Zool.* **41**, 1229-1240.

Cocroft, R. B., Tieu, T. D., Hoy, R. R. and Miles, R. N. (2000). Directionality in the directional response to substrate vibrations in a treehopper (Hemiptera: Membracidae: *Umbonia crassicornis*). *J. Comp. Physiol. A* **186**, 695-705.

Cooper, F. C. (1928). On the ear region of certain of the Chrysochloridae. *Philos. Trans. Soc. A Biol.* **216**, 265-283.

Ewing, W. M., Jardetzky, W. S. and Press, F. (1957). *Elastic Waves in Layered Media*. New York: McGraw-Hill.

Fielden, L. J. (1991). Home range movements of the Namib Desert golden mole, *Eremitalpa granti namibensis* (Chrysochloridae). *J. Zool. (Lond.)* **223**, 675-686.

Funnell, W. R. J., Siah, T. H., McKee, M. D., Daniel, S. J. and Decraemer, W. F. (2005). On the coupling between the incus and the stapes in the cat. *J. Assoc. Res. Otolaryngol.* **6**, 9-18.

Hartline, P. H. (1971). Physiological basis for detection of sound and vibration in snakes. *J. Exp. Biol.* **54**, 349-371.

Hetherington. T. E. (1989). The use of vibration cues for detection of insect prey by the sandswimming lizard *Scincus scincus. Anim. Behav.* **37**, 290-297.

Hill, P. S. M. and Shadley, J. R. (2001). Talking back: sending signals to lekking prairie mole cricket males. *Am. Zool.* **41**, 1200-1214.

Hyrtl, J. (1845). *Vergleichend-anatomiscche Untersuchungen über das Innere Gehörorgan des Menschen und der Säugetiere.* Prague: Friedrich Ehrlich Verlag.

Iida, K. (1938). The velocity of elastic waves in sand. *Bull. Earthq. Res. Inst. Univ. Tokyo* **16**, 131-145.

Iida, K. (1939). The velocity of elastic waves in granular substances. *Bull. Earthq. Res. Inst. Univ. Tokyo* **17**, 783-808.

Ishimoto, M. and Iida, K. (1937). Determinations of elastic constants of soil by means of vibration methods. Part II. Modulus of rigidity and Poisson's ratio. *Bull. Earthq. Res. Inst. Univ. Tokyo* **15**, 67-87.

Lewis, E. R. and Narins, P. M. (1985). Do frogs communicate with seismic signals? *Science* **227**, 187-189.

Lewis, E. R., Narins, P. M., Jarvis, J. U. M., Bronner, G. and Mason, M. J. (in press). Preliminary evidence for the use of microseismic cues for navigation by the Namib golden mole. *J. Acoust. Soc. Am.*

Mason, M. J. (1998). Functional anatomy of the middle ear of insectivores. *J. Acoust. Soc. Am.* **103**, 2827.

Mason, M. J. (2003a). Morphology of the middle ear of golden moles (Chrysochloridae). *J. Zool. (Lond.)* **260**, 391-403.

Mason, M. J. (2003b). Bone conduction and seismic sensitivity in golden moles (Chrysochloridae). *J. Zool. (Lond.)* **260**, 405-413.

Mason, M. J. and Narins, P. M. (2001). Seismic signal use by fossorial mammals. *Am. Zool.* **41**, 1171-1184.

Mason, M. J. and Narins, P. M. (2002). Seismic sensitivity in the desert golden mole (*Eremitalpa granti*). A review. *J. Comp. Psychol.* **116**, 158-163.

Michelsen, A. F., Fink, M., Gogala, M. and Traue, D. (1982). Plants as transmission channels for insect vibrational songs. *Behav. Ecol. Sociobiol.* **11**, 269-281.

Narins, P. M. (1990). Seismic communication in anuran amphibians. *Bioscience* **40**, 268-274.

Narins, P. M., Reichman, O. J., Jarvis, J. U. M. and Lewis, E. R. (1992). Seismic signal transmission between burrows of the Cape mole-rat, *Georychus capensis*. *J. Comp. Physiol. A* **170**, 13-21.

Narins, P. M., Lewis, E. R., Jarvis, J. U. M. and O'Riain, J. (1997). The use of seismic signals by fossorial southern African mammals: a neuroethological gold mine. *Brain Res. Bull.* **44**, 641-646.

O'Connell, C. E., Arnason, B. T. and Hart, L. A. (1997). Seismic transmission of elephant vocalizations and movement. *J. Acoust. Soc. Am.* **102**, 3124.

Rado, R., Levi, N., Hauser, H., Witcher, J., Adler, N., Intrator, N., Wollberg, Z. and Terkel, J. (1987). Seismic signaling as a means of communication in a subterranean mammal. *Anim. Behav.* **35**, 1249-1251.

Randall, J. A. and Lewis, E. R. (1997). Seismic communication between the burrows of kangaroo rats, *Dipodomys spectabilis*. *J. Comp. Physiol. A* **181**, 525-531.

Schön, F. and Müller, J. (1999). Measurements of the ossicular vibrations in the middle ear. *Audiol. Neurootol.* **4**, 142-149.

Sommerfeld, A. (1970). *Vorlesungen über Theoretische Physik II. Mechanik der Deformierbaren Medien*. Leipzig: Akademisch Verlagsgesellschaft Becker & Erler.

Von Dohlen, P. (1981). *Untersuchungen zum Vibrationssinn der Feldgrille*. PhD Thesis, Math. Sci. Fac., University of Cologne.

Von Meyer, A., O'Brien, G. and Sarmiento, E. E. (1995). Functional and systematic implications of the ear in golden moles (Chrysochloridae). *J. Zool. (Lond.)* **236**, 417-430.

Willi, U. B., Bronner, G. N. and Narins, P. M. (in press). Ossicular differentiation of airborne and seismic stimuli in the Cape golden mole (*Chrysochloris asiatica*). *J. Comp. Physiol. A.*